

RESEARCH

Open Access



Biogenic selenium nanoparticles induce ROS-mediated necroptosis in PC-3 cancer cells through *TNF* activation

Praveen Sonkusre and Swaranjit Singh Cameotra*

Abstract

Background: Selenium is well documented to inhibit cancer at higher doses; however, the mechanism behind this inhibition varies widely depending on the cell type and selenium species. Previously, we have demonstrated that *Bacillus licheniformis* JS2 derived biogenic selenium nanoparticles (SeNPs) induce non-apoptotic cell death in prostate adenocarcinoma cell line, PC-3, at a minimal concentration of 2 μg Se/ml, without causing toxicity to the primary cells. However, the mechanism behind its anticancer activity was elusive.

Results: Our results have shown that these SeNPs at a concentration of 2 μg Se/ml were able to induce reactive oxygen species (ROS) mediated necroptosis in PC-3 cells by gaining cellular internalization. Real-time qPCR analysis showed increased expression of necroptosis associated tumor necrotic factor (*TNF*) and interferon regulatory factor 1 (*IRF1*). An increased expression of RIP1 protein was also observed at the translational level upon SeNP treatment. Moreover, the cell viability was significantly increased in the presence of necroptosis inhibitor, Necrostatin-1.

Conclusion: Data suggest that our biogenic SeNPs induce cell death in PC-3 cells by the ROS-mediated activation of necroptosis, independent to RIP3 and MLKL, regulated by a RIP1 kinase.

Keywords: *Bacillus licheniformis* JS2, Biogenic selenium nanoparticles, PC-3, *TNF*, *IRF1*, Necroptosis, ROS, RIP1

Background

The treatment of cancer using nanoparticles is emerging as an alternative for cancer therapy. Nanoparticles provide site specific delivery of high drug load and thus reduce the risk of side effects and multidrug resistance in cancerous cells [1–3]. Since the drug delivery through NPs requires lower dose, it shows lower toxicity and offers increased half life to the carried drug molecule [4]. A diverse range of NPs have been synthesized and reported to have target specific enhanced anticancer activity. For example, the delivery of encapsulated PI3K inhibitor (BYL719) through fucoidan-based nanoparticles induced death in squamous cell carcinoma by preventing the side effects of hyperglycaemia [1]. Similarly, dendrimers or dendrimers- RNA triple helices conjugate were used as a nanoparticle to interact and adhere to the

tumors for the specific delivery of miRNA [5, 6]. Likewise, gold, lipid and lipopeptide nanoparticles were used for siRNA or drug delivery [7–9]. Thiolated-PEG-COOH functionalized gold nanoparticles were also reported to deliver biohybrid RNAi-peptide specifically to the cancer cells [10]. Similarly, various functionalized gold, platinum nanoparticles, quantum dots, lipidated particles, liposomes, and dendrimers have been used extensively for targeted drug delivery, imaging and cancer cell killing [11–16]. Among these nanomaterials, selenium nanoparticles (SeNPs) are reported to be the most promising nanosystem which itself has high anticancer activity and better biocompatibility [17, 18]. Every form of selenium is reported to have some anticancer activity with a different mechanism of action, and most of them are reported for prostate cancer inhibition. Selenite is reported to trigger caspase-mediated apoptosis in association with DNA fragmentation, phosphorylation of JNK1/2 and p38 MAPK/SAPK2 along with mitochondrial superoxide

*Correspondence: swaranjitsingh@yahoo.com; ssapplepie69@gmail.com
Institute of Microbial Technology, Sector 39 A, Chandigarh 160036, India

generation in PC-3 cells [19, 20]. It is also reported to cause the G2/M cell cycle arrest and induction of apoptosis in HCT116 and SW620 colorectal carcinoma cells through Bax-dependent mitochondrial pathway [21]. Similarly, methyl seleninic acid stimulates apoptosis in DU-145 human prostate carcinoma cells via PARP cleavage [22]. Selenomethionine causes downregulation of Bcl-xL along with up-regulation of Bax, Bad, Bim, and caspase-9 activation in SW480 tumor model [23]. It is also reported to stimulate apoptosis through p53 dependent cell cycle arrest in HCT116 and RKO colon cancer cells [24]. Nevertheless, chemically synthesized nanosized selenium is shown to induce cell cycle arrest, at S phase, in HeLa cells [25]. It inhibits the growth of LNCaP cells by suppressing the expression of androgen receptors at both transcriptional and translational levels, causes phosphorylation, ubiquitination-mediated degradation of androgen receptors through Akt/Mdm2 mediated pathway [26]. Transferrin-conjugated SeNPs prompt intracellular ROS production and activate MAPKs pathways to induce p53-mediated apoptosis in MCF-7 cells [17]. Glucose decorated SeNPs also reported to induce apoptosis in HepG2, MCF-7, A549 and Neuro-2a cells [18].

Due to the similar biological efficacy of SeNPs with that of inorganic and organic selenium; anticancer therapy using such particles is currently an extensively studied area. To overcome the issue of the lower therapeutic index of these selenium compounds, and to achieve enhanced biocompatibility and greater stability compared to the chemically synthesized SeNPs with an eco-friendly approach [17, 26, 27], we synthesized SeNPs biologically from *Bacillus licheniformis* JS2 strain and studied their cytotoxic effects on human prostate epithelial adenocarcinoma cells, PC-3.

Earlier, we have demonstrated that our biogenic SeNPs of an approximate size of 110 nm in diameter (Fig. 1a), induce non-apoptotic cell death in these cancer cells without affecting the viability of primary cells [human peripheral blood mononuclear cells (hPBMCs)] [28]. However, the intrinsic details were still elusive. Here, we have investigated the detailed mechanism underlying the cell death pathway. We observed an excellent *TNF* and ROS-mediated necroptosis in these cells at a minimal concentration of 2 μg Se/ml of SeNP (Fig. 1b).

Methods

Microorganism and culture conditions

Selenium nanoparticle synthesizing bacteria, *Bacillus licheniformis* JS2, isolated from the selenium-contaminated agricultural soil of Nawanshahr district (latitude 31°07' N and longitude 76°08' E) of Punjab, India, was used to synthesize SeNP aerobically [29].

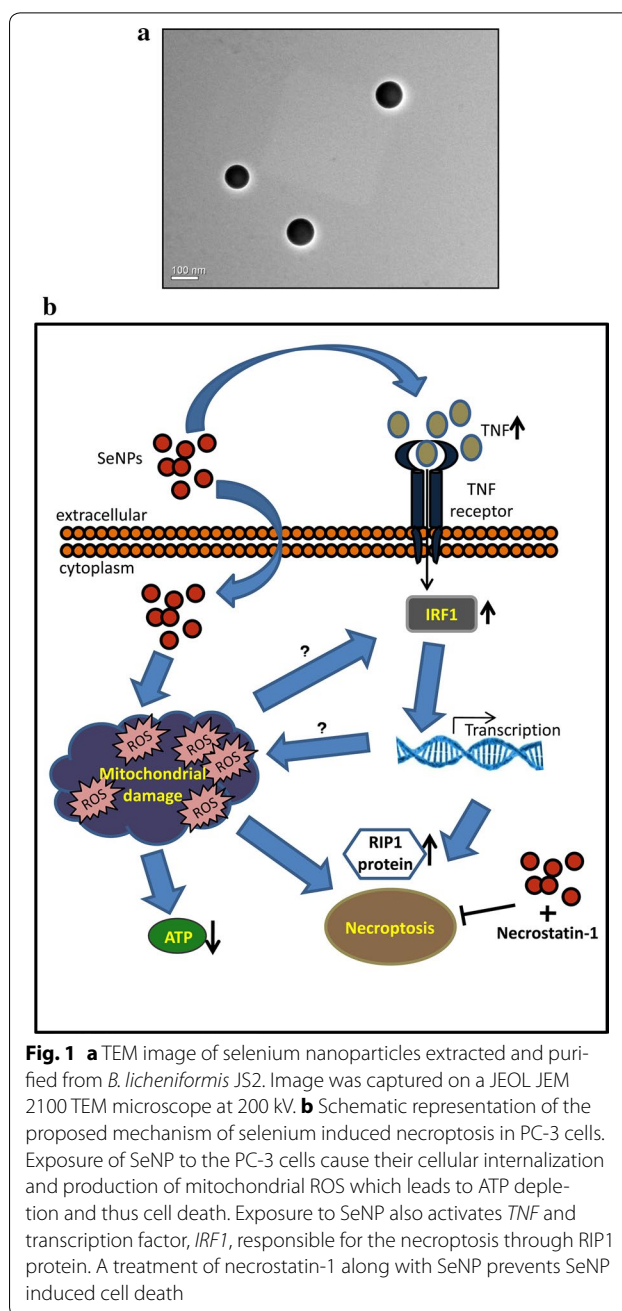


Fig. 1 **a** TEM image of selenium nanoparticles extracted and purified from *B. licheniformis* JS2. Image was captured on a JEOL JEM 2100 TEM microscope at 200 kV. **b** Schematic representation of the proposed mechanism of selenium induced necroptosis in PC-3 cells. Exposure of SeNP to the PC-3 cells cause their cellular internalization and production of mitochondrial ROS which leads to ATP depletion and thus cell death. Exposure to SeNP also activates *TNF* and transcription factor, *IRF1*, responsible for the necroptosis through RIP1 protein. A treatment of necrostatin-1 along with SeNP prevents SeNP induced cell death

Reagents

Tryptic soya broth (TSB) and agar (TSA) were procured from Hi-Media Laboratories. Sodium dodecyl sulfate (SDS), lysozyme, necrostatin-1, 3-(4,5-dimethylthiazol-2-yl)-2,5-diphenyltetrazolium bromide (MTT), metformin hydrochloride, 2-Deoxy-D-glucose, dihydrorhodamine 123, cytochalasin D, Durcupan™ ACM resin components; A, B, C, and D, triton X-100, absolute ethanol, and Bradford's reagent were purchased from Sigma-Aldrich. 1-octanol, tris-buffer, chloroform, HCl,

and luminata forte western HRP substrate were obtained from Merck-Millipore. Fetal bovine serum (FBS), TRIzol Reagent, and penicillin–streptomycin solution, and were purchased from Gibco-Invitrogen. CellTiter-Glo luminescent cell viability assay kit for ATP detection and CytoTox-ONE™ homogeneous membrane integrity assay kit for estimating LDH release were obtained from Promega and the manufacturer's instructions were followed. DyNAmo ColorFlash SYBR Green qPCR kit and Verso cDNA synthesis kit were procured from Thermo Fisher Scientific. RIP1, RIP3, and β -actin antibodies were purchased from Cell Signaling Technologies, MLKL, pMLKL, and pRIP3 were procured from Abcam. Secondary HRP antibodies were obtained from Santa Cruz Biotechnology. All plastic wares for cell culture were obtained from Nunc. Millipore water (Type II) was used in all the experiments.

Biosynthesis of selenium nanoparticle

Bacillus licheniformis JS2 strain was utilized for the synthesis of spherical SeNPs of an approximate size of 110 nm under aerobic condition in 1.8 mM sodium selenite stress. SeNPs were extracted and purified by following our previously reported method [28].

Quantification of selenium

Overnight acid digestion of SeNPs in 3:1 nitric acid: perchloric acid solution was performed and the samples were analyzed in a Shimadzu AA-6800 atomic absorption spectrophotometer (AAS) with selenium cathode lamp. Samples were atomized on acetylene flame and the selenium was quantified at 196 nm wavelength.

Cell lines and cell culture

A human prostate adenocarcinoma cell line (PC-3); derived from metastatic site, was purchased from the National Centre for Cell Science, Pune, India. Cells were cultured at 37 °C in a humidified incubator with 5% CO₂ in Ham's F-12K (Kaighn's) medium supplemented with 10% fetal bovine serum, 50 units/ml streptomycin, and 100 units/ml penicillin.

ATP depletion assay

PC-3 cells were seeded in 96-well opaque walled plate (white) at a density of 1×10^3 cells per well in Ham's F-12K (Kaighn's) medium supplemented with antibiotics and 10% FBS and kept at rest for 24 h at 37 °C in a humidified 5% CO₂ incubator. Cells were treated with SeNPs at a concentration of 2 μ g Se/ml and incubated further for 6 and 12 h at 37 °C. Cells treated with 5 mM metformin and 1 mM 2-deoxy-D-glucose were used as positive control for necrosis. CellTiter-Glo™ reagent was used according to the manufacturer's instructions to determine the levels of ATP present. The CellTiter-Glo™ Assay

generates a “glow-type” luminescent signal, produced by the luciferase reaction. The amount of luminescent signal corresponding to the levels of ATP was determined on a GloMax®-96 Microplate Luminometer.

Lactate dehydrogenase (LDH) release assay

PC-3 cells were seeded and kept on rest for 24 h as mentioned previously. Cells were treated with SeNPs at a concentration of 2 μ g Se/ml and incubated for another 12, 18, 24, or 30 h at 37 °C. LDH release from the cells, an indicator of membrane damage, was quantified using CytoTox-ONE™ assay kit. The assay is based on the conversion of non-fluorescent resazurin into the fluorescent resorufin product, directly proportional to the amount of LDH present. The levels of LDH were determined in the form of fluorescent signals on a BioTek Power Wave Microplate reader.

Dihydrorhodamine 123 (DHR123) staining and confocal microscopy

PC-3 cells were seeded onto sterile round 16 mm diameter glass coverslips in a 12-well tissue culture plate at a density of 2×10^5 cells per coverslip in Ham's F-12K (Kaighn's) medium supplemented with antibiotics and 10% FBS. Cells were kept at rest for 24 h at 37 °C in a 5% CO₂ incubator. After the rest period, cells were treated with SeNPs at a concentration of 2 μ g Se/ml and incubated for 16 h. Both SeNP treated and untreated cells were stained with 1 μ M DHR 123 for 30 min. After the incubation, the supernatant was discarded and the cells were washed 2–3 times with PBS (pH 7.4). Coverslips were placed inverted on the microscopic glass slides and visualized under Nikon A1R confocal microscope at 488 nm argon laser.

DHR123 staining and flow cytometry

2×10^5 cells per well were seeded in 12-well plates as detailed above. Cells were treated with SeNPs at a concentration of 2 μ g Se/ml and incubated for different time intervals, viz., 6, 9, 12, 15, 18, 21, or 24 h. Cells were stained with 1 μ M dihydrorhodamine 123 for 30 min, followed by harvesting with 10 mM EDTA solution. Harvested cells were washed twice with PBS (pH 7.4) and acquired in a BD AccuriC6 Flow Cytometer (BD Biosciences). The data analysis was performed by FlowJo software.

Cytochalasin D treatment

PC-3 cells were seeded in 12-well plates at a density of 2×10^5 cells per well as mentioned previously. After 24 h, test wells were treated with 2 μ M cytochalasin D for 30 min. The medium was discarded; adhered cells were rinsed and supplemented with 1 ml of fresh Ham's

F-12K (Kaighn's) medium. Cells were treated with SeNPs at a concentration of 2 $\mu\text{g Se/ml}$ and incubated for 16 h at 37 °C in a CO₂ incubator. Cells were harvested, and an AnnexinV-FITC Apoptosis Detection Kit was used to stain the cells with FITC labeled annexinV and propidium iodide according to the manufacturer's instructions. Cells were acquired in a BD AccuriC6 Flow Cytometer (BD Biosciences). The data analysis was performed by FlowJo software.

In another set, cells were stained with 1 μM dihydrorhodamine 123 for 30 min before harvesting. Harvested cells were washed 2–3 times with PBS (pH 7.4) and acquired in a BD AccuriC6 Flow Cytometer (BD Biosciences). The data analysis was performed by FlowJo software.

Block preparation and TEM analysis

To confirm the cellular internalization of SeNPs, TEM analysis of PC-3 cells was performed after 12 h treatment with SeNP. PC-3 cells were seeded in a 6 well plate at a density of 5×10^5 cells per well and kept at rest for 24 h at 37 °C. After the rest period, cells were treated with SeNPs at a concentration of 2 $\mu\text{g Se/ml}$, and incubated for 12 h. Cells were harvested using 10 mM EDTA solution and washed thrice with PBS. 700 μl of Karnovsky's fixative was added and the samples were fixed for 3 h at 4 °C. Samples were stained, dehydrated, and embedded as per the standard protocol using Durcupan™ ACM resin components; A, B, C and D (Sigma-Aldrich). Ultrathin sections of 70 nm thickness were prepared using a Leica EM UC7 ultramicrotome. Samples were collected on copper grids and visualized at 200 kV on a JEOL JEM-2100 TEM microscope after negative staining.

RNA extraction

PC-3 cells were seeded in 6-well plates at a density of 5×10^5 cells as mentioned earlier. After the rest period, cells were treated with SeNPs at a concentration of 2 or 4 $\mu\text{g Se/ml}$ and incubated for 16 h. Cells were rinsed with PBS and harvested using TRIzol reagent. Harvested cells were lysed by multiple pipetting (15–20 times) followed by 5 min incubation at RT. 150 μl of chloroform was added, mixed by inversion (approx. 15 times) and kept undisturbed at RT for another 5 min. Samples were centrifuged at 10,000 $\times g$ for 15 min at 4 °C. Approximate 200 μl of the upper aqueous layer from each microcentrifuge tube (MCT) was carefully transferred to the respective fresh diethyl pyrocarbonate (DEPC) treated MCT and an equal volume of isopropanol was added. Samples were gently mixed by inverting the tubes 4–5 times followed by 10 min incubation at room temperature (RT). After the incubation, RNA-containing samples were centrifuged at 14,000 $\times g$ for 10 min at 4 °C. Supernatants

were discarded and the pellets were washed twice with 70% ethanol at 10,000 $\times g$ for 5 min at 4 °C. Each MCT containing the RNA pellet was allowed to dry at RT, and the dried pellets were resuspended in 20 μl of nuclease free water.

cDNA synthesis and quantitative Real Time PCR

Extracted RNA were quantified on nanodrop (Thermo Scientific), 1000 ng of each sample was reverse transcribed using a Verso cDNA synthesis kit (Thermo Fisher Scientific) according to the manufacturer's instruction. cDNA was amplified by Eppendorf MasterCycler RealPlex⁴ PCR with gene specific primers using the DyNAmo ColorFlash SYBR Green qPCR kit (Thermo Fisher Scientific). Housekeeping gene, β -actin, was used as an internal control. The relative fold change was calculated by using formula $2^{-\Delta\Delta\text{Ct}}$.

Necroptosis inhibition

Necrostatin-1 was used to inhibit SeNPs induced necroptosis in PC-3 cells. 3.5×10^3 cells per well were seeded in Ham's F-12K (Kaighn's) medium in 96-well flat bottom cell culture plates. After the resting period of 24 h, cells were subjected with 2 $\mu\text{g Se/ml}$ SeNPs or, 2 $\mu\text{g Se/ml}$ SeNPs and necrostatin-1 (20 μM , or 50 μM) or DMSO, and cultured for 24 h at 37 °C. 10 μl of (5 mg/ml) MTT [3-(4,5-dimethylthiazol-2-yl)-2,5-diphenyltetrazolium bromide] solution was added to each well, and the plates were incubated for 3.5 h at 37 °C. 80 μl of the solubilizing solution, 20% SDS (w/v) in 50% DMF (v/v), was added to each well in a sterile condition. The plates were kept at 37 °C for 3 h at 120 rpm. 130 μl from each well was transferred into a fresh 96 well plate and analyzed on a BioTek Power Wave Microplate reader at 570 nm. Production of the violet colored formazan in this assay corresponds to the cell viability.

Protein extraction and western blotting

PC-3 cells were seeded in 6-well plates at a density of 5×10^5 cells as mentioned earlier. Cells were then subjected with SeNPs at a concentration of 2 $\mu\text{g Se/ml}$, or 4 $\mu\text{g Se/ml}$, or 2 $\mu\text{g Se/ml}$ with Nec-1 (50 μM), or 4 $\mu\text{g Se/ml}$ with Nec-1 (50 μM), and incubated for 12 h. Cells were rinsed with PBS and harvested in cell lysis buffer [150 mM NaCl, 50 mM Tris-Cl (pH 7.4), 2 mM EDTA, 1 mM dithiothreitol (DTT), 4 mM Na₃VO₄, 1% triton-X 100, and 1% glycerol], containing protease inhibitor cocktail. Protein content was estimated using Bradford's reagent. 30 μg protein samples were separated on 10% sodium dodecyl sulfate–polyacrylamide gel electrophoresis (SDS-PAGE) followed by protein transfer to polyvinylidene difluoride (PVDF) membrane. After blocking with 5% BSA, membranes were incubated overnight

with primary antibodies (anti-MLKL, anti-phospho MLKL, anti-phospho RIP3, anti-β-actin, anti-RIP1, and anti-RIP3 antibodies), followed by incubation with HRP-conjugated secondary antibodies. Luminata Forte Western HRP substrate (Millipore) was used for the blot development.

Statistical analysis

All the experiments were performed at least in triplicates and presented here as their mean ±SD. GraphPad Prism 6 software was used for all the statistical analysis. Statistical significances were calculated using the unpaired Student’s *t* test.

Results

Biogenic SeNPs causes mitochondrial damage without affecting the cell membrane integrity

Intracellular ATP levels were determined after SeNP treatment. Cells treated for 6 or 12 h with 2 μg Se/ml SeNP show a significant decrease in the levels of cellular ATP compared to the control cells, suggesting the mitochondrial damage (Fig. 2a).

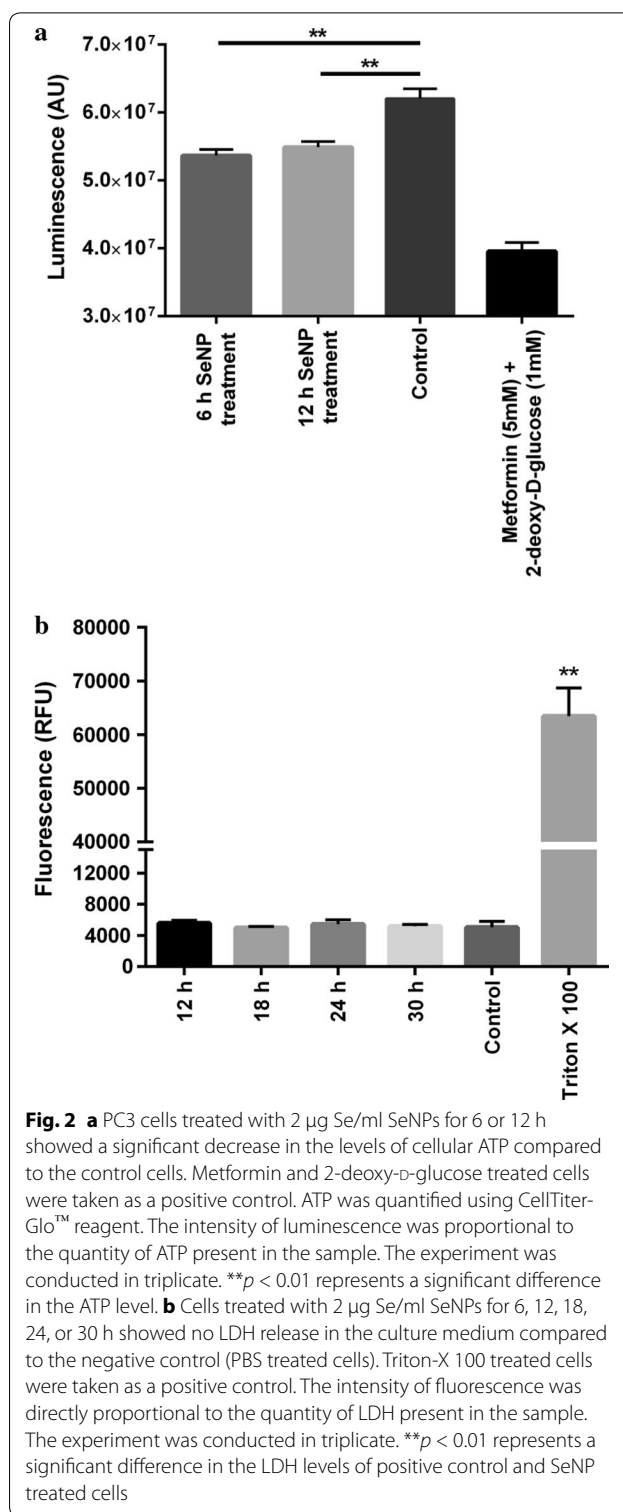
The levels of LDH were also estimated by using CytoTox-ONE homogeneous membrane integrity assay kit (Promega). No significant increase in the LDH level was observed in the culture medium after treating cells with 2 μg Se/ml SeNP for 12, 18, 24, or 30 h compared to the untreated cells (Fig. 2b).

SeNP stimulates ROS production after gaining cellular internalization

As selenium is reported to cause oxidative stress, levels of reactive oxygen species (ROS) were measured at different time intervals after SeNP treatment using a non-fluorescent molecule dihydrorhodamine 123. Dihydrorhodamine 123 which can passively diffuse across the membrane converted into a fluorescent probe rhodamine 123 in the presence of ROS and localize into the mitochondria which were detected by confocal microscopy and quantified in FACS. Confocal microscopy performed after 12 h of SeNPs treatment showed the presence of fluorescent rhodamine 123 in the form of puncta as an indicator of mitochondrial ROS (Fig. 3).

The time-dependent change in the levels of mitochondrial ROS was also estimated via FACS. Results indicated that the production of ROS increased gradually, it was maximum at 15 h of treatment and then decreased gradually as the number of viable cells decreased (Fig. 4a). A clear shift in the cell population was started appearing after 12 h of treatment in comparison to untreated cells (Fig. 4b).

To confirm that the cytotoxicity is caused by the cellular internalization (endocytosis) of SeNPs, cells were



treated with cytochalasin D (an inhibitor of actin polymerization which is known to block endocytosis and >90% of the phagocytosis [30]) prior to SeNP treatment. FACS analysis of AnnexinV-FITC and propidium iodide

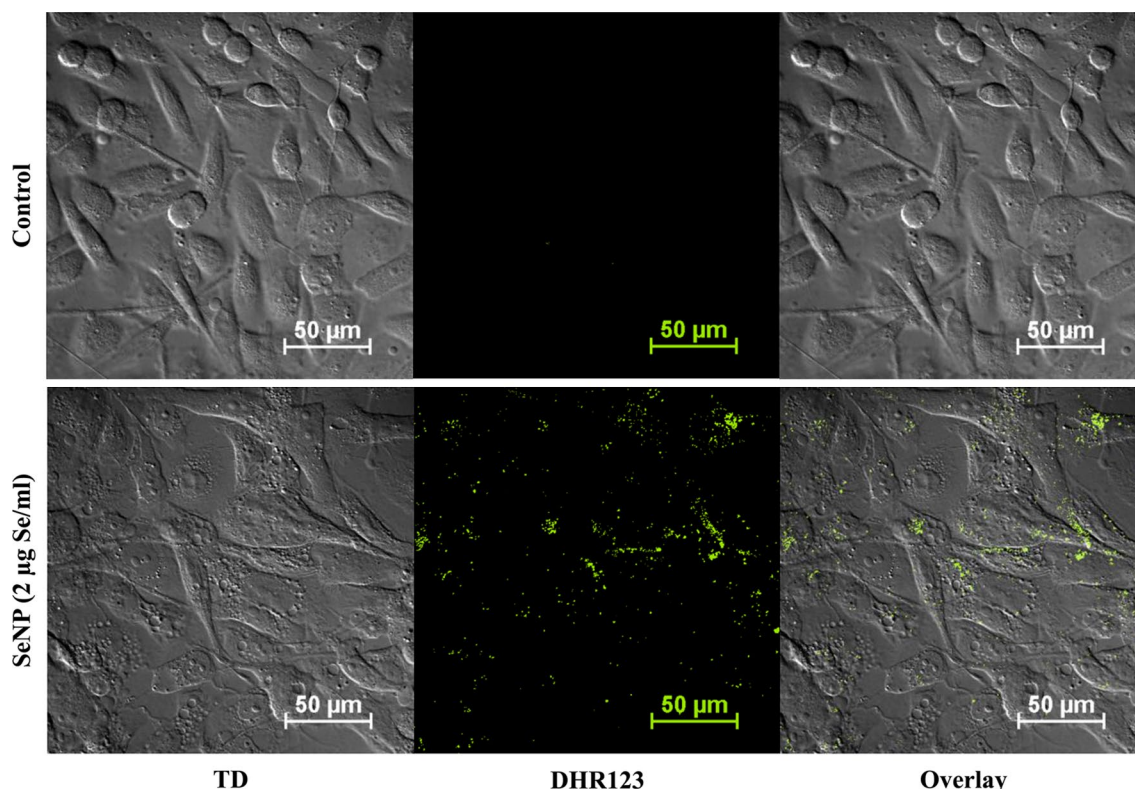


Fig. 3 Biogenic SeNPs induce ROS-mediated cytotoxicity in PC-3 cancer cells. 24 h cultured PC-3 cancer cells were treated with SeNPs at a concentration of 2 µg Se/ml for 12 h. Mitochondrial ROS were visualized using dihydrorhodamine 123 at 60× oil immersion under the confocal microscope with 488 nm argon laser. ROS-induced cleavage of dihydrorhodamine 123 produces a fluorescent molecule, rhodamine 123, which was evident in the form of *greenish yellow* colored puncta

or DHR123 stained cells after 16 h of SeNP treatment showed more viability with less ROS production in cells treated with cytochalasin D, compared to cytochalasin D untreated cells (Fig. 5a, b). This suggested that toxicity caused by the selenium nanoparticles in PC-3 cells is due to their cellular internalization.

Endocytosis of SeNPs was confirmed by visualizing their intracellular localization under transmission electron microscope (TEM) by preparing ultrathin sections of SeNP treated PC-3 cells using an ultramicrotome. NPs were mostly found to be located in the cytoplasm (Fig. 5c).

SeNP induces overexpression of necroptotic genes

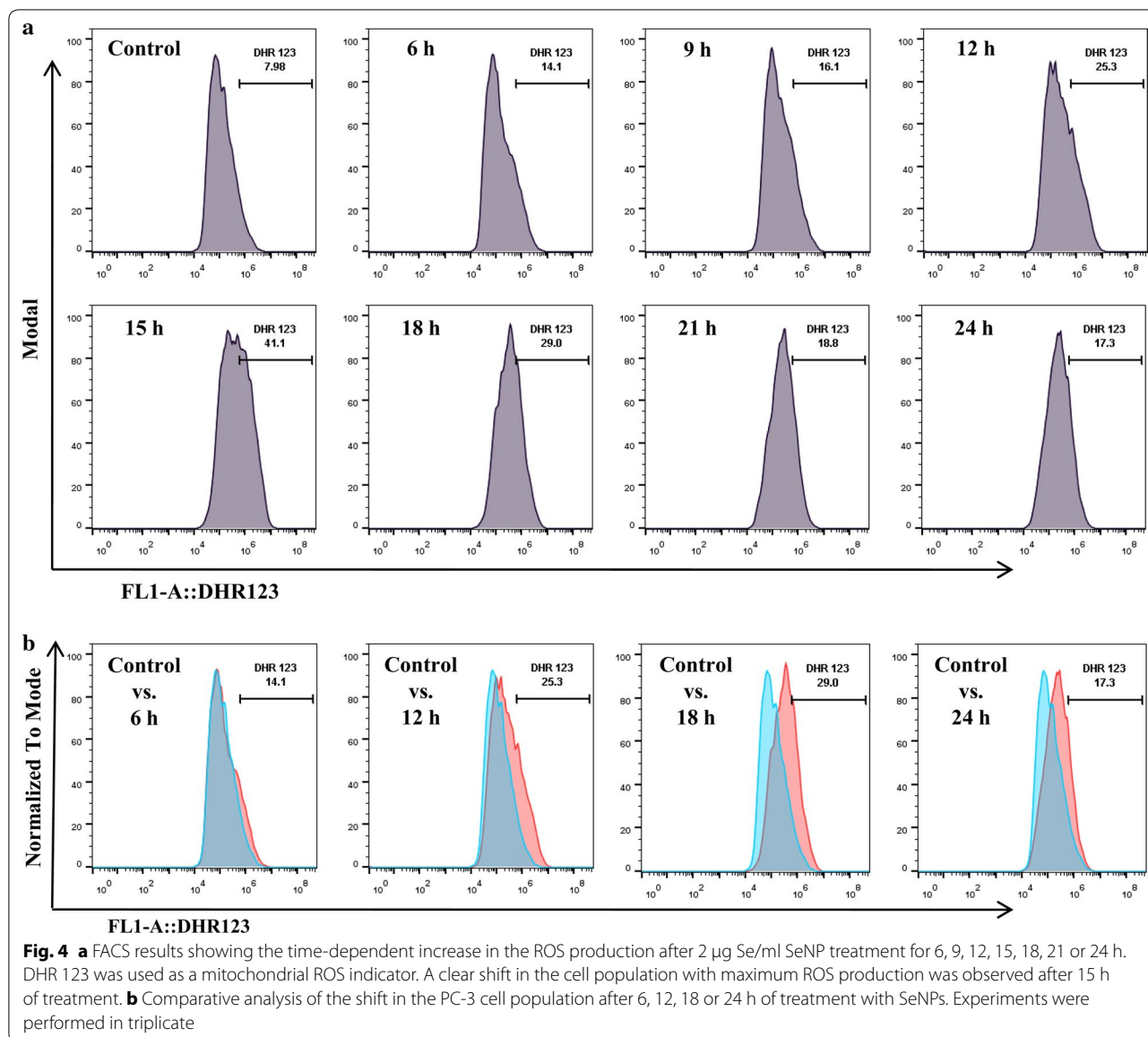
To identify the pathway involved in cell death, real-time mRNA expression analysis was performed. Expression of characteristic molecules from different cell death pathway was studied in a real-time PCR. A dose-dependent overexpression of only *TNF* and *IRF1* mRNA was observed in SeNP treated cells. More than twofolds or fourfolds increase was observed in the expression of *TNF*

and *IRF1* mRNA under 2 µg or 4 µg Se/ml SeNP stress, respectively (Fig. 6).

SeNP induces RIP3 independent necroptosis in PC-3 cells

Since necroptosis is reported to be coupled with the phosphorylation of RIP3 and MLKL, we performed western blot analysis to estimate the phosphorylated and unphosphorylated status of these proteins. Results showed no expression of RIP3 as well as its phosphorylated form in both SeNP treated and untreated cells. Furthermore, no change in MLKL expression and the absence of its phosphorylated form was observed in control as well as SeNP treated cells. However, SeNP dependent significant increase in the RIP1 protein expression was evident. The treatment of Nec-1 along with SeNP did not affect expression pattern of any of the protein (Fig. 7a).

The viability of SeNP treated cells cultured in the presence or absence of necroptosis inhibitor, Necrostatin-1, was determined in an MTT assay. A significant relative increase in the cell viability was observed in wells



supplemented with Nec-1. The viability was directly proportional to the concentration of Nec-1 added (Fig. 7b).

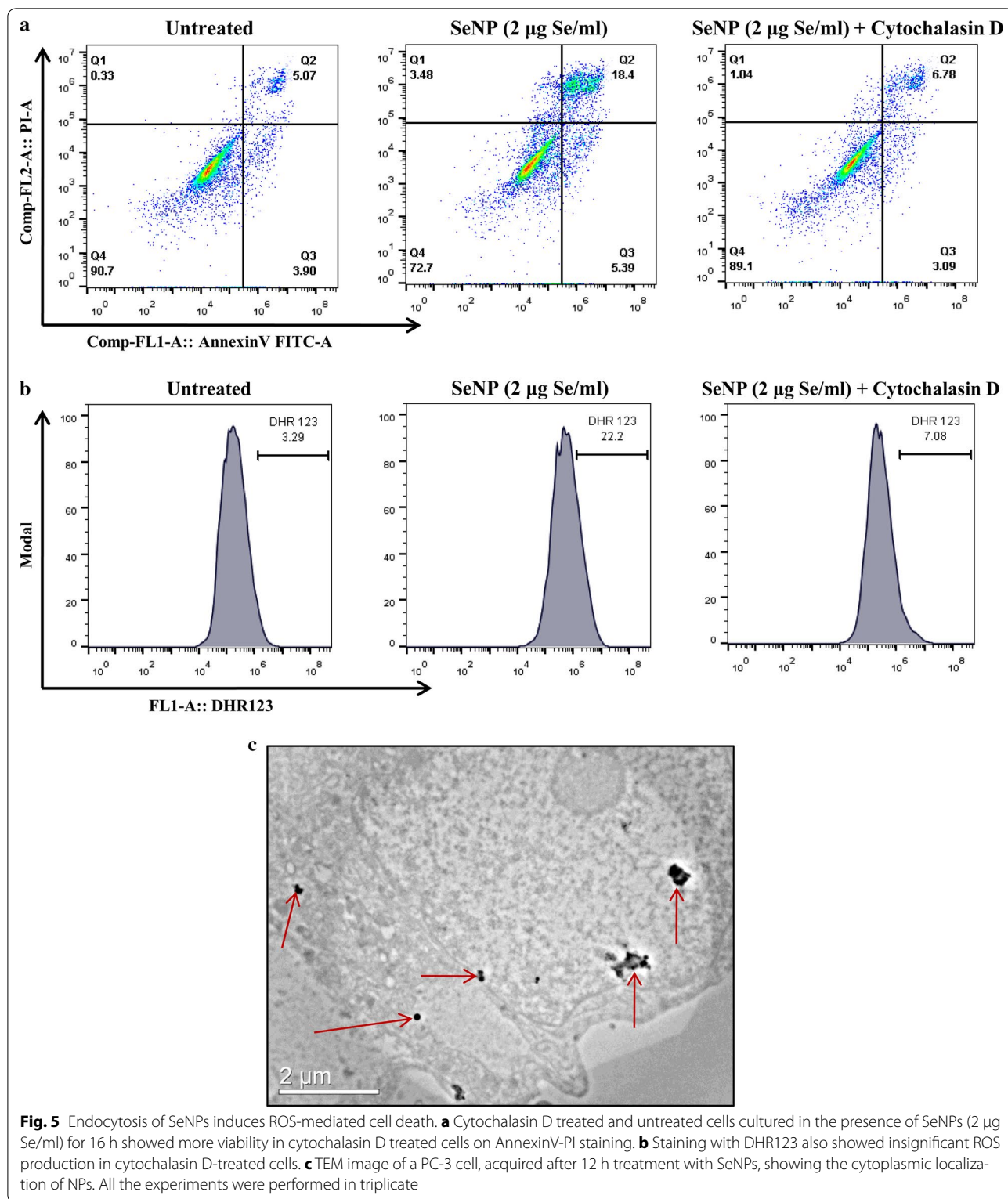
Discussion

Every form of selenium has more or less anticancer activity and it is typically observed in prostate, colon and lung cancer [31–37]. However, the anticancer properties depend on the selenium species, dose, cancer type and stage [32]. It can be affected by the environmental factors, genotype and the bioavailability of selenium. The mode and extent of cell death vary widely depending on the selenium species. Several mechanisms have been suggested for the anticancer activity of selenium, including cell cycle arrest, antioxidation, apoptosis, interruption of cell signaling pathway [17–20, 25, 38] etc. Recently,

SeNPs came into limelight because of their excellent anti-cancer activity with lower toxicity compared to the other inorganic and organic forms of selenium [27, 39–41] and thus, emerging as a potential cancer chemopreventive agent.

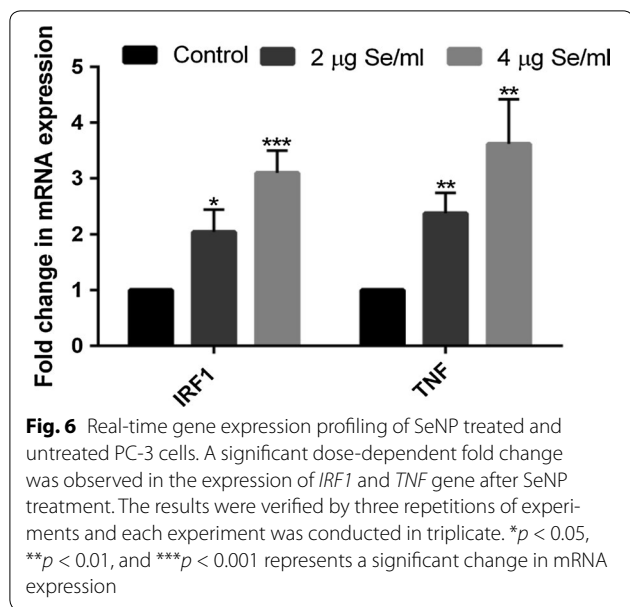
In our previous study, we have demonstrated that a minimum concentration of only 2 μg Se/ml of these, ~110 nm in diameter, well characterized, *B. licheniformis* derived, sterically stabilized SeNP is very effective in inhibiting the proliferation and inducing mortality in PC-3 cancer cells through a caspase-independent pathway [28].

In this present report, we have analyzed the underlying mechanism behind the SeNP mediated PC-3 cell death. A significant depletion in the ATP levels was observed



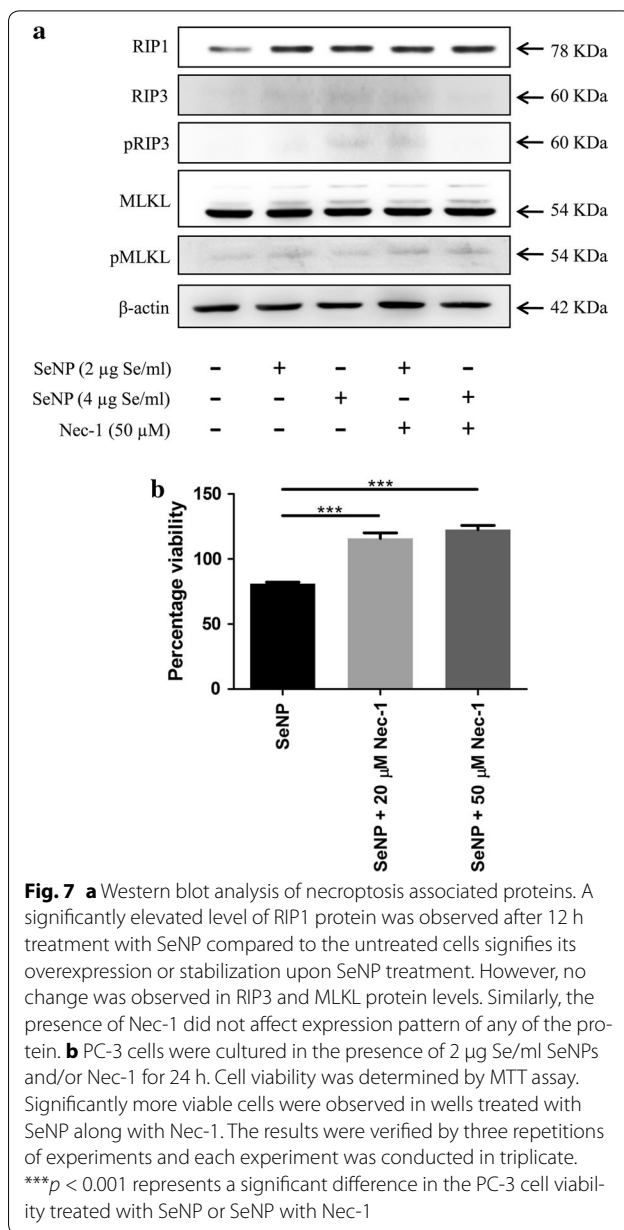
within 6 h of SeNP treatment, supporting the phenomenon of necrosis/necroptosis [42]. As LDH release is a hallmark feature of necrotic/necroptotic cell death, we

have studied the LDH release upon SeNP treatment. Surprisingly, there was no LDH release observed in the culture medium even after 30 h of treatment.



We also observed endocytosis of SeNPs that leads to the drastic production of mitochondrial ROS. ROS generation along with ATP depletion indicated the SeNP induced mitochondrial damage. A significant increase in the levels of *TNF* and *IRF1* gene expression was also observed in qPCR. *IRF1* is a well-known transcription activator of the genes induced by interferons α , β , and γ thereby inhibits the cell growth and suppresses tumor progression. Previous studies suggested that production of ROS and the activation of *TNF* and *IRF1* genes are involved in the induction of regulated necrosis (necroptosis) [43–46]. Reactive oxygen species of mitochondrial origin are also extensively documented in necroptotic cell death [46–48]. Conversely, glucose decorated and transferrin conjugated SeNPs were reported to cause apoptosis by the induction of caspase 3, 8 and 9 and mitochondrial ROS. However, in this study PC-3 cells did not show any sign of apoptosis under SeNPs treatment. This is probably because our SeNPs have different surface, size and structural properties compared to the earlier reports. SeNPs are reported to have different mechanisms of cell death depending on the mode of synthesis, the presence of functional groups, bioavailability, size, structure (lattice arrangement of atoms), and compactness of the NPs [17, 18, 25–27]. This variability is largely observed when chemical and biological syntheses of NPs are compared. These changes play a tremendous role in their biological activity [49–52].

According to the literature, the conventional pathway of necroptosis is triggered by a number of inflammatory signals like *TNF* α and TLRs [53]. The process is independent of caspases and is initiated through a necrosome



complex containing RIP1 and RIP3 kinases. Necroptotic cell death is dependent on the phosphorylation of MLKL through RIPK3. MLKL is an essential necroptosis effector molecule downstream to the RIP1/RIP3 complex, which after phosphorylation migrates and localized to the plasma membrane and compromises its integrity that in turn releases intracellular proinflammatory molecules [54–56].

However, our western blot results showed no expression of RIP3 and no MLKL phosphorylation. This declined the possibility of necrosome formation and indicates that biogenic SeNP induced cell death is not

activated through a conventional RIP3–MLKL necroptosis pathway. In support of our results, the literature also suggests, most of the cancer cell lines, including the PC-3 cells, do not express RIP3 due to the methylation-dependent gene silencing [57, 58]. However, we have observed a significant increase in RIP1 expression at the protein level after SeNP treatment. Though, a similar change was not observed at mRNA level (date not shown), suggesting that probably SeNP treatment is stabilizing the RIP1 protein, responsible for the cell death, possibly due to post-translational modification(s) which can be explored further.

We also observed no effect of Nec-1 on the MLKL, pMLKL, RIP1, RIP3, and pRIP3 expression. However, a significant increase in the cell viability was observed on Nec-1 treatment, suggesting the role of RIP1 in SeNP induced cell death. In support of our results, RIP3 and MLKL independent necroptosis is also reported in the literature [59–61].

Here, necroptosis does not involve pMLKL, and probably because of which we have not observed membrane damage. As per our knowledge, necroptosis event with the formation of RIP1/RIP3 complex is shown only in the RIP3 expressing cells. Here we suggest the possibility of SeNP induced RIP3/MLKL independent necroptosis downstream to the RIP1 in RIP3 non-expressing PC-3 cells.

Conclusion

We summarize our study with a conclusion that *B. licheniformis* derived sterically stabilized biogenic SeNP at a minimum concentration of 2 µg Se/ml cause *TNF* and *IRF1* induced ROS-mediated necroptosis, in PC-3 cells. The event is observed dependent to the RIP1, however, independent of the RIP3 and the activation of MLKL and thus independent of the necrosome complex formation. Further studies can be done to identify the events and molecules involved in this necroptosis pathway mediated by the RIP1 kinase.

Abbreviations

AAS: atomic absorption spectrophotometer; ATP: adenosine triphosphate; BSA: bovine serum albumin; DEPC: diethyl pyrocarbonate; DHR 123: dihydro rhodamine 123; DMF: dimethylformamide; EDTA: ethylenediaminetetraacetic acid; FACS: fluorescence activated cell sorting; FITC: fluorescein isothiocyanate; HRP: horseradish peroxidase; IRF1: interferon regulatory factor 1; LDH: lactate dehydrogenase; MCT: microcentrifuge tube; MLKL: mixed lineage kinase domain-like protein; MTT: 3-(4,5-dimethylthiazol-2-yl)-2,5-diphenyltetrazolium bromide; Nec-1: necrostatin-1; PBMCs: human peripheral blood mononuclear cells; pMLKL: phosphorylated form of MLKL; pRIP3: phosphorylated form of RIP3; PVDF: polyvinylidene difluoride; qPCR: quantitative real-time PCR; RIP1: receptor-interacting serine/threonine-protein kinase 1; RIP3: receptor-interacting serine/threonine-protein kinase 3; ROS: reactive oxygen species; RT: room temperature; SD: standard deviation; SDS-PAGE: sodium dodecyl sulfate–polyacrylamide gel electrophoresis; SeNP: elemental selenium nanoparticles;

TSA: tryptic soya agar; TSB: tryptic soya broth; TEM: transmission electron microscope; TNFα: tumor necrotic factor alpha; TLRs: toll-like receptors.

Authors' contributions

PS designed and performed the experiments and contributed to the manuscript preparation. SSC provided valuable suggestions, contributed to manuscript preparation, and supervised the project. Both authors read and approved the final manuscript.

Acknowledgements

We are thankful to Dr. Pawan Gupta for providing resources and working space in his cell culture facility. Thanks also go to Dr. Ravikanth Nanduri for necessary discussions. We are also grateful to the Director, Institute of Microbial Technology—a constituent laboratory of Council of Scientific and Industrial Research (CSIR), for providing excellent infrastructure and facility. P.S. thank CSIR for providing fellowship.

Competing interests

The authors declare that they have no competing interests.

Availability of data and materials

The datasets used and/or analyzed during the current study available from the corresponding author on reasonable request.

Publisher's Note

Springer Nature remains neutral with regard to jurisdictional claims in published maps and institutional affiliations.

Received: 9 February 2017 Accepted: 22 May 2017

Published online: 07 June 2017

References

- Mizrachi A, Shamay Y, Shah J, Brook S, Soong J, Rajasekhar VK, Humm JL, Healey JH, Powell SN, Baselga J, et al. Tumour-specific PI3K inhibition via nanoparticle-targeted delivery in head and neck squamous cell carcinoma. *Nat Commun*. 2017;8:14292.
- Biju V. Chemical modifications and bioconjugate reactions of nanomaterials for sensing, imaging, drug delivery and therapy. *Chem Soc Rev*. 2014;43:744–64.
- Ranganathan R, Madanmohan S, Kesavan A, Baskar G, Krishnamoorthy YR, Santosham R, Ponraju D, Rayala SK, Venkatraman G. Nanomedicine: towards development of patient-friendly drug-delivery systems for oncological applications. *Int J Nanomed*. 2012;7:1043–60.
- Banerjee D, Sengupta S. Nanoparticles in cancer chemotherapy. *Prog Mol Biol Transl Sci*. 2011;104:489–507.
- Khan OF, Zaia EW, Jhunjhunwala S, Xue W, Cai W, Yun DS, Barnes CM, Dahlman JE, Dong Y, Pelet JM, et al. Dendrimer-inspired nanomaterials for the in vivo delivery of siRNA to lung vasculature. *Nano Lett*. 2015;15:3008–16.
- Conde J, Oliva N, Atilano M, Song HS, Artzi N. Self-assembled RNA-triple-helix hydrogel scaffold for microRNA modulation in the tumour microenvironment. *Nat Mater*. 2016;15:353–63.
- Conde J, Oliva N, Zhang Y, Artzi N. Local triple-combination therapy results in tumour regression and prevents recurrence in a colon cancer model. *Nat Mater*. 2016;15:1128–38.
- Dong Y, Love KT, Dorkin JR, Sirirungruang S, Zhang Y, Chen D, Bogorad RL, Yin H, Chen Y, Vegas AJ, et al. Lipopeptide nanoparticles for potent and selective siRNA delivery in rodents and nonhuman primates. *Proc Natl Acad Sci USA*. 2014;111:3955–60.
- Resnier P, Galopin N, Sibiril Y, Clavreul A, Cayon J, Briganti A, Legras P, Vessieres A, Montier T, Jaouen G, et al. Efficient ferrocifen anticancer drug and Bcl-2 gene therapy using lipid nanocapsules on human melanoma xenograft in mouse. *Pharmacol Res*. 2017. doi:10.1016/j.phrs.2017.01.031.

10. Conde J, Bao C, Tan Y, Cui D, Edelman ER, Azevedo HS, Byrne HJ, Artzi N, Tian F. Dual targeted immunotherapy via in vivo delivery of biohybrid RNAi-peptide nanoparticles to tumour-associated macrophages and cancer cells. *Adv Funct Mater*. 2015;25:4183–94.
11. Hou X, Yang C, Zhang L, Hu T, Sun D, Cao H, Yang F, Guo G, Gong C, Zhang X, et al. Killing colon cancer cells through PCD pathways by a novel hyaluronic acid-modified shell-core nanoparticle loaded with RIP3 in combination with chloroquine. *Biomaterials*. 2017;124:195–210.
12. Ali MR, Wu Y, Han T, Zang X, Xiao H, Tang Y, Wu R, Fernandez FM, El-Sayed MA. Simultaneous time-dependent surface-enhanced raman spectroscopy, metabolomics, and proteomics reveal cancer cell death mechanisms associated with gold nanorod photothermal therapy. *J Am Chem Soc*. 2016;138:15434–42.
13. Jawaid P, Rehman MU, Hassan MA, Zhao QL, Li P, Miyamoto Y, Misawa M, Ogawa R, Shimizu T, Kondo T. Effect of platinum nanoparticles on cell death induced by ultrasound in human lymphoma U937 cells. *Ultrason Sonochem*. 2016;31:206–15.
14. Conde J, Tian F, Hernandez Y, Bao C, Baptista PV, Cui D, Stoeger T, de la Fuente JM. RNAi-based glyconanoparticles trigger apoptotic pathways in vitro and in vivo enhanced cancer-cell killing. *Nanoscale*. 2015;7:9083–91.
15. Suganya KS, Govindaraju K, Kumar VG, Karthick V, Parthasarathy K. Pectin mediated gold nanoparticles induces apoptosis in mammary adenocarcinoma cell lines. *Int J Biol Macromol*. 2016;93:1030–40.
16. Child HW, Hernandez Y, Conde J, Mullin M, Baptista P, de la Fuente JM, Berry CC. Gold nanoparticle-siRNA mediated oncogene knockdown at RNA and protein level, with associated gene effects. *Nanomedicine (Lond)*. 2015;10:2513–25.
17. Huang Y, He L, Liu W, Fan C, Zheng W, Wong YS, Chen T. Selective cellular uptake and induction of apoptosis of cancer-targeted selenium nanoparticles. *Biomaterials*. 2013;34:7106–16.
18. Nie TQ, Wu HL, Wong KH, Chen TF. Facile synthesis of highly uniform selenium nanoparticles using glucose as the reductant and surface decorator to induce cancer cell apoptosis. *J Mater Chem B*. 2016;4:2351–8.
19. Chen P, Wang L, Li N, Liu Q, Ni J. Comparative proteomics analysis of sodium selenite-induced apoptosis in human prostate cancer cells. *Metalomics*. 2013;5:541–50.
20. Xiang N, Zhao R, Zhong W. Sodium selenite induces apoptosis by generation of superoxide via the mitochondrial-dependent pathway in human prostate cancer cells. *Cancer Chemother Pharmacol*. 2009;63:351–62.
21. Li Z, Meng J, Xu TJ, Qin XY, Zhou XD. Sodium selenite induces apoptosis in colon cancer cells via Bax-dependent mitochondrial pathway. *Eur Rev Med Pharmacol Sci*. 2013;17:2166–71.
22. Jiang C, Wang Z, Ganther H, Lu J. Caspases as key executors of methyl selenium-induced apoptosis (anoikis) of DU-145 prostate cancer cells. *Cancer Res*. 2001;61:3062–70.
23. Yang Y, Huang F, Ren Y, Xing L, Wu Y, Li Z, Pan H, Xu C. The anticancer effects of sodium selenite and selenomethionine on human colorectal carcinoma cell lines in nude mice. *Oncol Res*. 2009;18:1–8.
24. Goel A, Fuerst F, Hotchkiss E, Boland CR. Selenomethionine induces p53 mediated cell cycle arrest and apoptosis in human colon cancer cells. *Cancer Biol Ther*. 2006;5:529–35.
25. Luo H, Wang F, Bai Y, Chen T, Zheng W. Selenium nanoparticles inhibit the growth of HeLa and MDA-MB-231 cells through induction of S phase arrest. *Colloids Surf B Biointerfaces*. 2012;94:304–8.
26. Kong L, Yuan Q, Zhu H, Li Y, Guo Q, Wang Q, Bi X, Gao X. The suppression of prostate LNCaP cancer cells growth by Selenium nanoparticles through Akt/Mdm2/AR controlled apoptosis. *Biomaterials*. 2011;32:6515–22.
27. Zhang J, Wang X, Xu T. Elemental selenium at nano size (Nano-Se) as a potential chemopreventive agent with reduced risk of selenium toxicity: comparison with se-methylselenocysteine in mice. *Toxicol Sci*. 2008;101:22–31.
28. Sonkusre P, Nanduri R, Gupta P, Cameotra SS. Improved extraction of intracellular biogenic selenium nanoparticles and their specificity for cancer chemoprevention. *J Nanomed Nanotechnol*. 2014;5:194–202.
29. Dhanjal S, Cameotra SS. Selenite stress elicits physiological adaptations in *Bacillus* sp. (strain JS-2). *J Microbiol Biotechnol*. 2011;21:1184–92.
30. Ribes S, Ebert S, Regen T, Agarwal A, Tauber SC, Czesnik D, Spreer A, Bunkowski S, Eiffert H, Hanisch UK, et al. Toll-like receptor stimulation enhances phagocytosis and intracellular killing of nonencapsulated and encapsulated *Streptococcus pneumoniae* by murine microglia. *Infect Immun*. 2010;78:865–71.
31. Brinkman M, Reulen RC, Kellen E, Buntinx F, Zeegers MP. Are men with low selenium levels at increased risk of prostate cancer? *Eur J Cancer*. 2006;42:2463–71.
32. Etmann M, FitzGerald JM, Gleave M, Chambers K. Intake of selenium in the prevention of prostate cancer: a systematic review and meta-analysis. *Cancer Causes Control*. 2005;16:1125–31.
33. Vogt TM, Ziegler RG, Graubard BI, Swanson CA, Greenberg RS, Schoenberg JB, Swanson GM, Hayes RB, Mayne ST. Serum selenium and risk of prostate cancer in U.S. blacks and whites. *Int J Cancer*. 2003;103:664–70.
34. Donaldson MS. Nutrition and cancer: a review of the evidence for an anti-cancer diet. *Nutr J*. 2004;3:19.
35. Finley JW, Davis CD, Feng Y. Selenium from high selenium broccoli protects rats from colon cancer. *J Nutr*. 2000;130:2384–9.
36. Clark LC, Combs GF Jr, Turnbull BW, Slate EH, Chalker DK, Chow J, Davis LS, Glover RA, Graham GF, Gross EG, et al. Effects of selenium supplementation for cancer prevention in patients with carcinoma of the skin. A randomized controlled trial. Nutritional Prevention of Cancer Study Group. *JAMA*. 1996;276:1957–63.
37. Zhuo P, Diamond AM. Molecular mechanisms by which seleno-proteins affect cancer risk and progression. *Biochim Biophys Acta*. 2009;1790:1546–54.
38. Dong Y, Lee SO, Zhang H, Marshall J, Gao AC, Ip C. Prostate specific antigen expression is down-regulated by selenium through disruption of androgen receptor signaling. *Cancer Res*. 2004;64:19–22.
39. Wang H, Zhang J, Yu H. Elemental selenium at nano size possesses lower toxicity without compromising the fundamental effect on selenoenzymes: comparison with selenomethionine in mice. *Free Radic Biol Med*. 2007;42:1524–33.
40. Zhang JS, Gao XY, Zhang LD, Bao YP. Biological effects of a nano red elemental selenium. *BioFactors*. 2001;15:27–38.
41. Zhang J, Wang H, Yan X, Zhang L. Comparison of short-term toxicity between Nano-Se and selenite in mice. *Life Sci*. 2005;76:1099–109.
42. Zamaraeva MV, Sabirov RZ, Maeno E, Ando-Akatsuka Y, Bessonova SV, Okada Y. Cells die with increased cytosolic ATP during apoptosis: a bioluminescence study with intracellular luciferase. *Cell Death Differ*. 2005;12:1390–7.
43. McComb S, Cessford E, Alturki NA, Joseph J, Shutinoski B, Startek JB, Gamero AM, Mossman KL, Sad S. Type-I interferon signaling through ISGF3 complex is required for sustained Rip3 activation and necroptosis in macrophages. *Proc Natl Acad Sci USA*. 2014;111:E3206–13.
44. Sosna J, Voigt S, Mathieu S, Lange A, Thon L, Davarnia P, Herdegen T, Linkermann A, Rittger A, Chan FK, et al. TNF-induced necroptosis and PARP-1-mediated necrosis represent distinct routes to programmed necrotic cell death. *Cell Mol Life Sci*. 2014;71:331–48.
45. Wajant H, Pfizenmaier K, Scheurich P. Tumor necrosis factor signaling. *Cell Death Differ*. 2003;10:45–65.
46. Lin Y, Choksi S, Shen HM, Yang QF, Hur GM, Kim YS, Tran JH, Nedospasov SA, Liu ZG. Tumor necrosis factor-induced nonapoptotic cell death requires receptor-interacting protein-mediated cellular reactive oxygen species accumulation. *J Biol Chem*. 2004;279:10822–8.
47. Vanlangenakker N, Vanden Berghe T, Bogaert P, Laukens B, Zobel K, Deshayes K, Vucic D, Fulda S, Vandennebeele P, Bertrand MJ. cIAP1 and TAK1 protect cells from TNF-induced necrosis by preventing RIP1/RIP3-dependent reactive oxygen species production. *Cell Death Differ*. 2011;18:656–65.
48. Marshall KD, Baines CP. Necroptosis: is there a role for mitochondria? *Front Physiol*. 2014;5:323.
49. Oh WK, Kim S, Choi M, Kim C, Jeong YS, Cho BR, Hahn JS, Jang J. Cellular uptake, cytotoxicity, and innate immune response of silica-titania hollow nanoparticles based on size and surface functionality. *ACS Nano*. 2010;4:5301–13.
50. Kim ST, Saha K, Kim C, Rotello VM. The role of surface functionality in determining nanoparticle cytotoxicity. *Acc Chem Res*. 2013;46:681–91.
51. Moghadam BY, Hou WC, Corredor C, Westerhoff P, Posner JD. Role of nanoparticle surface functionality in the disruption of model cell membranes. *Langmuir*. 2012;28:16318–26.
52. Asati A, Santra S, Kaittanis C, Perez JM. Surface-charge-dependent cell localization and cytotoxicity of cerium oxide nanoparticles. *ACS Nano*. 2010;4:5321–31.
53. Belizario J, Vieira-Cordeiro L, Enns S. Necroptotic Cell Death Signaling and Execution Pathway: lessons from Knockout Mice. *Mediators Inflamm*. 2015;2015:128076.

54. Dondelinger Y, Declercq W, Montessuit S, Roelandt R, Goncalves A, Bruggeman I, Hulpiau P, Weber K, Sehon CA, Marquis RW, et al. MLKL compromises plasma membrane integrity by binding to phosphatidylinositol phosphates. *Cell Rep*. 2014;7:971–81.
55. Cai Z, Jitkaew S, Zhao J, Chiang HC, Choksi S, Liu J, Ward Y, Wu LG, Liu ZG. Plasma membrane translocation of trimerized MLKL protein is required for TNF-induced necroptosis. *Nat Cell Biol*. 2014;16:55–65.
56. Wang H, Sun L, Su L, Rizo J, Liu L, Wang LF, Wang FS, Wang X. Mixed lineage kinase domain-like protein MLKL causes necrotic membrane disruption upon phosphorylation by RIP3. *Mol Cell*. 2014;54:133–46.
57. Murphy JM, Vince JE. Post-translational control of RIPK3 and MLKL mediated necroptotic cell death. *F1000 Res*. 2015. doi:[10.12688/f1000research.7046.1](https://doi.org/10.12688/f1000research.7046.1).
58. Koo GB, Morgan MJ, Lee DG, Kim WJ, Yoon JH, Koo JS, Kim SI, Kim SJ, Son MK, Hong SS, et al. Methylation-dependent loss of RIP3 expression in cancer represses programmed necrosis in response to chemotherapeutics. *Cell Res*. 2015;25:707–25.
59. Christofferson DE, Yuan J. Necroptosis as an alternative form of programmed cell death. *Curr Opin Cell Biol*. 2010;22:263–8.
60. Degtrev A, Huang Z, Boyce M, Li Y, Jagtap P, Mizushima N, Cuny GD, Mitchison TJ, Moskowitz MA, Yuan J. Chemical inhibitor of nonapoptotic cell death with therapeutic potential for ischemic brain injury. *Nat Chem Biol*. 2005;1:112–9.
61. Shulga N, Pastorino JG. GRIM-19-mediated translocation of STAT3 to mitochondria is necessary for TNF-induced necroptosis. *J Cell Sci*. 2012;125:2995–3003.

Submit your next manuscript to BioMed Central and we will help you at every step:

- We accept pre-submission inquiries
- Our selector tool helps you to find the most relevant journal
- We provide round the clock customer support
- Convenient online submission
- Thorough peer review
- Inclusion in PubMed and all major indexing services
- Maximum visibility for your research

Submit your manuscript at
www.biomedcentral.com/submit

